

Enabling Verification of Deep Neural Networks in Perception Tasks Using Fuzzy Logic and Concept Embeddings

Gesina Schwalbe^{1,2}[0000–0003–2690–2478], Christian Wirth¹, and Ute Schmid²[0000–0002–1301–0326]

¹ Continental AG, Regensburg, Germany

`gesina.schwalbe@conti.de`

`christian.2.wirth@continental-corporation.com`

² Cognitive Systems, University of Bamberg, Bamberg, Germany

`ute.schmid@uni-bamberg.de`

Abstract. One major drawback of deep convolutional neural networks (CNNs) for use in safety critical applications is their black-box nature. This makes it hard to verify or monitor complex, symbolic requirements on already trained computer vision CNNs. In this work, we present a simple, yet effective, approach to verify that a CNN complies with symbolic predicate logic rules which relate visual concepts. It is the first that (1) does not modify the CNN, (2) may use visual concepts that are no CNN in- or output feature, and (3) can leverage continuous CNN confidence outputs. To achieve this, we newly combine methods from explainable artificial intelligence and logic: First, using supervised concept embedding analysis, the output of a CNN is post-hoc enriched by concept outputs. Second, rules from prior knowledge are modelled as truth functions that accept the CNN outputs, and can be evaluated with little computational overhead. We here investigate the use of fuzzy logic, i.e., continuous truth values, and of proper output calibration, which both theoretically and practically show slight benefits. Applicability is demonstrated on state-of-the-art object detectors for three verification use-cases, where monitoring of rule breaches can reveal detection errors.

Keywords: Concept Activation Vectors, Fuzzy Logic, Calibration, Verification, Runtime Monitoring, CNN, XAI

1 Introduction

Deep neural network (DNN) debugging and safety critical use-cases like automated driving perception require verification of semantic prior domain knowledge [32]. Such knowledge relates concepts that are semantically meaningful to humans, e.g., objects, sub-objects, and object properties, and is potentially complex and fuzzy [25]. Examples are physical laws or typical anatomical structures.

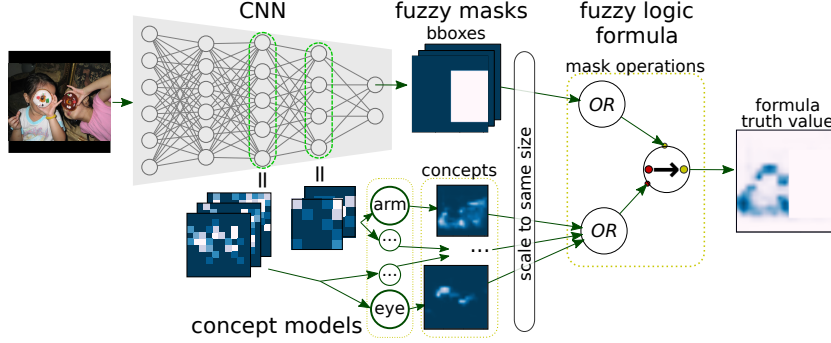


Fig. 1: Visualization of our approach from Sec. 3 for the pixel-wise formula $F(p) = (\text{Is}_{\text{eye}}(p) \vee \text{Is}_{\text{arm}}(p) \vee \dots) \rightarrow \text{Is}_{\text{Person}}(p)$. (Image attribution in Fig. 2).

While it would be desirable to formulate the prior knowledge as verifiable constraints, this fails for standard black-box object detection CNNs for computer vision tasks [21]. In particular, they lack an association of semantic concepts with inputs or (intermediate) outputs: (1) inputs are non-symbolic, (2) final outputs only describe few concepts to reduce labeling costs (e.g., few object classes, no sub-object classes), and (3) intermediate outputs are non-interpretable. Hence, standard work on improving [6] or formally verifying [20] rule compliance are not applicable without custom-built DNN architectures. One way to overcome this and post-hoc extract learned concept information from a trained CNN is concept (embedding) analysis (CA) [3,7,13]. The idea is to attach cheap and small models to the CNN intermediate outputs. These are trained in a supervised manner to predict the existence of a concept. This also works for large object detectors as shown in [31], requires only few additional labels [7,12], and leaves the original DNN unchanged.

We here combine CA with methods of (fuzzy) formal rule formulation. This for the first time allows to *post-hoc* score the compliance of CNN outputs *and intermediate outputs* with *predicate logic rules*, such as formalizations of “Limbs usually belong to a person”. For this, the outputs of a CNN are interpreted as family of logical predicates that produce (fuzzy) truth values from image inputs. Rules are modelled to be truth functions accepting these truth values and yielding pixel- or region-wise *logical consistency scores*. Once the rule model is established, the evaluation works in a *self-supervised* manner, suitable for several debugging and verification use-cases: (1) identification of corner cases (examples with low score), (2) comparison of the logical consistency of different CNNs, and (3) monitoring of logical consistency as error indicator during runtime.

Besides the mentioned use-cases, this work investigates the benefits of using t-norm *fuzzy logic* [25] for modelling, and of *calibrating* the newly attached CNN outputs. Fuzzy logic promises to better leverage the continuity of CNN outputs [11]. And, for a mathematically sound interpretation as truth values, CNN outputs should be calibrated (cf. Sec. 3.3). Our contributions are:

- (i) A novel, simple, extensible and scalable framework to construct a *truth value monitor* for logical constraints on semantic concepts (Sec. 3, cf. Fig. 1),
- (ii) Development and comparison of *modeling options for formulating the monitor*, including different fuzzification methods (Secs. 3.1 and 4.2),
- (iii) Analysis of benefits from *model calibration* and *fuzziness*,
- (iv) Demonstration on two *state-of-the-art object detectors* and two safety relevant occlusion robustness rules for pedestrian detection (Sec. 4.2);
- (v) We show that the framework can *uncover a substantial proportion of detection errors* with a single rule.

2 Related Work

Fuzzy Logic Integration into DNNs: Diligenti et al. [5] suggested to use fuzzy logic rules as loss functions for DNN training, relying on continuous t-norm fuzzy logic [25]. This inclusion of semantic prior knowledge to the training was shown to bring significant performance improvements for different types of rules [30,24,2], and was extended to several frameworks [23,2]. While we build upon this idea, the prior work requires all referenced concepts to be features in the DNN output, and does not guarantee that classifier outputs are calibrated.

Concept Embedding Analysis: The basic works from CA associate semantic concepts with linear combinations (*concept activation vectors*) of neurons [13] or CNN filters [7]. For this, small linear *concept models* are attached to CNN intermediate outputs. We use the successor [31] of [7] as part of our framework (cf. Sec. 3.2), but apply calibration and optimize the choice of loss towards this. Prior work proposes two semantic consistency metrics based on CA: correct similarity between concept encodings [7,31], and attribution of early-layer concepts to later-layer ones [13,34]. Both are restricted in the complexity of verifiable relations, whereas this work can deal with general predicate logic rules.

Calibration: For obtaining calibrated confidence estimates, we use model calibration. Common post-calibration methods [9] are computationally cheap, but approximate Bayesian learning is usually outperforming these methods [16]. However, common variational inference methods [15] are mostly restricted to a mean field approximation, disregarding the covariance, due to computational cost. Hence, we use a full covariance Laplace approximation [17], as this is computationally viable with our approach. Find a comprehensive overview in [1].

Other Monitoring Approaches: Self-supervised runtime monitoring of DNNs usually relies on uncertainty estimation, like [29], or consistency checks based on pixel-attribution or additional inputs, e.g. LiDAR. Uncertainty can detect outliers or proximity to decision boundaries [26], but no logical inconsistencies. Pixel-attribution can be used to check for spurious input attribution patterns of the model [8,18], or for attention not local to detected objects [4]. While this is useful for manual inspection, attention methods are restricted in the rules that can be checked, and inference of our method requires only a single forward pass.

3 Approach

Assume one wants to verify that an object detector respects the rule “Heads and limbs belong to a person” formalized to the predicate logic formula F

$$F(p) := \text{IsBodyPart}(p) \rightarrow \text{IsPartOfAPerson}(p) \quad (1)$$

$$\text{with } \text{IsPartOfAPerson}(p) := (\exists q \in P: \text{Is}_{\text{person}}(q) \wedge \text{CloseBy}(p, q)) \quad (2)$$

$$\text{and } \text{IsBodyPart}(p) := \bigvee_{b \in \text{BodyParts}} \text{Is}_b(p) \quad (3)$$

with the free variable $p \in \text{Images} \times \text{PixelPositions}$ a pixel position in an image, and some pre-defined **BodyParts** predicates Is_b for $b \in \text{BodyParts}$. Such a formula with free variables can be viewed as a function on the variable values that outputs a single truth value for “Is the rule fulfilled”. It can be modeled as computational tree with the nodes being functions and logical operations, i.e. logical conjunctions \vee, \wedge, \neg ; quantifiers \forall, \exists ; and predicates like $\text{Is}_{\text{person}}$. The main idea for verifying a rule on CNN outputs is to interpret the CNN as family of predicates, i.e., functions that output truth values. We dissect the formula evaluation into the following steps (cf. Fig. 1):

1. **Obtain outputs of predicates** (calibrated, Sec. 3.3) and functions:
 - Predicates describing a CNN output, like $\text{Is}_{\text{person}}$: derived from CNN output.
 - Predicates describing internal knowledge of the CNN, like Is_{arm} : extracted from the activation maps via concept analysis (Sec. 3.2).
2. **Evaluate the residual computational tree of the formula** to obtain a final (fuzzy) truth value.

To leverage the knowledge encoded in the confidences of the DNN outputs, we also consider to *fuzzify* all logical operations (Sec. 3.1). It should be noted that all components (additional concept outputs, Sec. 3.2; calibration, Sec. 3.3; rule evaluation) only require few standard tensor operations, and thus produce negligible computational overhead.

3.1 Fuzzy Logic on DNN Outputs

For fuzzification of logical operations, we rely on the theory of t-norm fuzzy logic [25]. We first recapitulate needed basics thereof. Then, further modeling aspects for fuzzy rules are detailed, and the considered applications.

Basics of Fuzzy Logic Fuzzy logic generalizes standard predicate logic by allowing more than two truth values. This concerns the logical operations, which are the following: *Logical connectives* **NOT** (\neg), **AND** (\wedge), **OR** (\vee), and *implication* (\rightarrow) reduce one or several truth values to a single truth value. *Quantifiers* **all** (\forall), and *exists* (\exists) reduce a given domain of values (e.g. pixel positions) to a single truth value using a body formula. *Predicates* take symbol values (constants or instantiated variables), and return a single truth value. For example, predicates arising from DNN confidence outputs are inherently fuzzy. Intuitive

fuzzy logical connectives may be defined using a t-norm fuzzy logic [25]. The t-norm fuzzy logics from Tab. 1 represent a generating basis of all t-norm logics with continuous *AND* [25, sec. 2.3.1, p. 48]. Quantifiers can either be naturally expressed via the chosen logical connectives by $(\forall x \in X: F(x)) := (\bigwedge_{x \in X} F(x))$ and $(\exists x \in X: F(x)) := (\bigvee_{x \in X} F(x))$, or be implemented by a mean operation, as suggested in [6].

Notation: Predicates with binary output are underlined.

Table 1: The fuzzy connectives *AND* (*t-norm*), *OR* (*t-conorm*), *residuated implication* (R-implication) and *strong implication* (S-implication) defined by Boolean logic (Bool) and standard t-norm fuzzy logics Łukasiewicz (L), Goedel/Minimum (G), and Product/Goguen (P). Bool applies the standard Boolean operations to values binarized at a threshold $\tau = \tau_{\text{Bool}}$ (default: 0.5).

	Negation	Conjunction	Disjunction	R-Implication	S-Implication
Logic	$\neg a$	$a \wedge b$	$a \vee b$	$a \rightarrow_R b$	$(\neg a) \vee b$
L	$1 - a$	$\max(0, a + b - 1)$	$\min(1, a + b)$	$\min(1, 1 - a + b)$	$\min(1, 1 - a + b)$
G	$1 - a$	$\min(a, b)$	$\max(a, b)$	1 if $a \leq b$ else b	$\max(1 - a, b)$
P	$1 - a$	$a \cdot b$	$a + b - a \cdot b$	$\min(1, \frac{b}{a})$	$1 - a + a \cdot b$
Bool	$\neg(a \geq \tau)$	$(a \geq \tau) \wedge (b \geq \tau)$	$(a \geq \tau) \vee (b \geq \tau)$	$(a < \tau) \vee (b \geq \tau)$	$(a < \tau) \vee (b \geq \tau)$

Formulation of Rules for Object Detection Object detection is subject to several fuzzy logic rules that are based, e.g., on laws, physical constraints, or statistical prior knowledge like typical anatomy. Simple examples are spatial rules, e.g., “Road users usually do not fly.”, or “A person located on top of a bike is usually a cyclist.”; and hierarchical rules, e.g., “Cars usually have wheels.”, or the example rule from Eq. (1). Note that the last one describes a safety relevant occlusion robustness: Infringements of the rule may indicate that the detector can fail in cases of high occlusion when only few body parts are visible. To leverage pixel-wise information obtained from the DNN, we propose a pixel-wise formulation of rules, as done in the example rule from Eq. (1). This allows to model the logical operations via few standard tensor operations on the mask tensors. Further details of our modeling approach are given in the following.

For **fuzzy connectives** we consider the three t-norm fuzzy logics detailed in Tab. 1. Note that the non-continuous R-implication $a \rightarrow_R b$ of product and Goedel logic is instable if truth values of both a and b are small [2]. As baseline we consider non-fuzzy Boolean logic, where \wedge and \vee translate to standard mask intersection and union. For this, all inputs to logical connectives must be binarized at a threshold τ_{Bool} (default 0.5). This may reduce memory consumption, but discards potentially valuable confidence information.

In [6], the **fuzzy quantifier** definition $\forall = \text{mean}$ was suggested as an intuitive and differentiable implementation. Note that, other than \forall quantifiers

derived from a fuzzy *OR*, mean gives rise to the following inequality for a subset $Q \subset P$ and a t-norm fuzzy implication:

$$(\forall p \in Q: F(p)) \neq (\forall p \in P: (p \in Q) \rightarrow F(p)) \quad (4)$$

The right hand formulation produces generally large values for small Q ³. Thus, to keep intuition intact, we recommend the left hand formulation from (4) where applicable. When choosing the \exists quantifier, it must be noted that for $\forall = \text{mean}$ the standard definition $(\exists x: F(x)) = (\neg \forall x: \neg F(x))$ for a formula body F would produce $\exists = \text{mean}$. This ignores high truth values when their proportion in the domain is too low. Thus, a \exists defined from a fuzzy logic \wedge is preferable.

Typical **predicates** occurring in rules for object detection are unary concept predicates (“Does the concept apply to the location/region?”) and spatial relations. Using examples from Eq. (1), we demonstrate different ways to model predicates: using predicted or ground truth (GT) bounding boxes (e.g., $\text{Is}_{\text{person}}$, $\text{Is}_{\text{GTPerson}}$), using concept segmentation masks (e.g., IsBodyPart), and manually (e.g., CloseBy).

Box information. Instance-wise bounding box information for an object class can be turned into a fuzzy semantic segmentation mask, e.g., with the following simplistic transformation: (1) Each bounding box is turned into a mask by setting pixels inside the bounding box to their bounding box objectness score value, and (2) if needed, the box masks are combined using pixel-wise logical *OR* of the respective fuzzy logic. For GT bounding boxes, the objectness score may be set constant to 1.

Segmentation masks. Segmentation outputs, e.g. from CA (here called *concept masks*, cf. Sec. 3.2), can serve as unary concept predicates, each pixel value being a truth value for a pixel position. The masks of different concepts may differ in resolution, e.g. those from CA have the resolution of CNN activation maps. To ensure compatible sizes, one can: (a) upscale masks to the common largest resolution, e.g. bilinearly [31], or (b) downscale masks to the common smallest resolution, e.g. using maxpooling⁴.

CloseBy. We suggest two formulations of a spatial close-by relations on pixel coordinates a, b , a Gaussian radial distance function (with a low cut for memory efficiency), and a simpler binary one that checks L_1 proximity:

$$\text{CloseBy}_{\sigma, r}(a, b) := \exp(-d(a, b)^2 / (2\sigma^2)) \quad (5)$$

$$\text{CloseBy}(p, q) := (\|p - q\|_1 \leq \lfloor \frac{1}{2}(\text{ksize} - 1) \rfloor), \quad (6)$$

with $d(a, b) := \|a - b\|_2$ if $\|a - b\|_1 \leq r$ for a window half size r , else 0. CloseBy_{σ} becomes trivial if $\sigma = 0$, i.e., $\text{CloseBy}_0(a, b) = 1$ if $a \equiv b$ else 0. Note that CloseBy can be defined from a neighborhood definition $\text{Nbh}(\cdot)$ via set membership: $\text{CloseBy}(p, q) = (q \in \text{Nbh}(p))$ (cf. Eq. (4)). For Eq. (6) $\text{Nbh}(p)$ is a

³ $(\forall p \in P: (p \in Q) \rightarrow F(p)) = \frac{\#P - \#Q}{\#P} + \frac{\#Q}{\#P} \text{mean}_{p \in Q} F(p)$

⁴ Formally, maxpooling on a unary predicate Is_x can be written as $\exists p' \in P': \text{CloseBy}(p, p') \wedge \text{Is}_x(p')$ for a pixel $p \in P$ on some other resolution P' , and binary $\text{CloseBy}(p, p') = (\|p - p'\|_1 \leq \lfloor \frac{1}{2}(\text{ksize} - 1) \rfloor)$ (cf. Eq. (8)).

square window of size \mathbf{ksize} around p . A non-trivial spatial relation may help to mitigate segmentation mask resolution problems: Upscaling low resolution masks may cause positive regions to become too large. For example, in the rule from Eq. (1) body part masks may “shoot over” the person areas, leading to rule infringements at person area boundaries (cf. Fig. 2).

One **pattern** for rule formulation we consider here is that of a neighborhood prior for pixel-wise formulas F . The neighbor condition $\mathbf{NbCond}_F(p, P)$ should down-weight $F(p)$ if it is spatially isolated (noise) within the region P . We suggest to score p isolated if none (Eq. (8)) or, alternatively, not all (Eq. (7)) of p ’s neighbors have a high $F(p)$ value, formally:

$$\mathbf{NbCond}_F(p, P) = \forall q \in P: \mathbf{CloseBy}(p, q) \rightarrow F(q) \stackrel{\text{binary}}{\underset{\text{CloseBy}}{=}} \forall q \in \mathbf{Nb}(p): M(q) \quad (7)$$

$$\mathbf{NbCond}_F(p, P) = F(p) \wedge (\exists q \in P \setminus \{p\}: \mathbf{CloseBy}(p, q) \wedge F(q)) \quad (8)$$

If $\mathbf{CloseBy}$ is radial symmetric, Eq. (7) selects center points of radial peaks. For $\mathbf{CloseBy}$ defined via a square \mathbf{Nb} as in Eq. (6), and using Eq. (4) and $\forall = \text{mean}$, the neighborhood condition Eq. (7) can be efficiently implemented as a stride 1 average pooling. In this case, to not loose any peak, the kernel size \mathbf{ksize} is best chosen to cover at least the minimum expected area of an interesting peak.

Fuzzy Rules for Verification Assume one is given a logical rule of the form $R(P) = \forall p \in P: F(p)$ where the variable P is an image or image region, and $p \in P$ means a pixel position in that region, and F a truth function on such valid pixels $p \in \text{ImageRegions} \times \text{PixelPositions}$, like in Eq. (1). For a concrete image, the pixel outputs of F together form a mask with values in $[0, 1]$ that are high where the formula is fulfilled, and low otherwise. R yields for an image or image region P a single truth value that can be interpreted as a logical consistency score for P . We suggest the following use-cases to utilize R and F for verification, given a test set T .

Corner Case Search: R can be evaluated for each image in T . Outliers with respect to the consistency score distribution may serve as pre-selection for manual analysis in order to identify root causes of illogical behavior.

Global Logical Consistency Score: The aggregation $\forall P \in T: R(P)$ of image-wise scores over T yields a global consistency score over T . The score allows, e.g., comparison of different networks trained on the same dataset, or comparison of different training datasets.

Monitoring: The pixel-wise truth scores given by F give rise to several runtime monitoring scenarios. For our example formula Eq. (1), a monitor would have the task to reveal cases of detector false negatives where some body part was found but no person predicted in the end. A *pixel-wise monitor* that observes whether pixels p have a suspiciously low truth value can be defined as

$$M(p) := \neg F(p) \in [0, 1]. \quad (9)$$

Alarm is raised if an inconsistency bound is breached, i.e., $M(p) \geq \mathbf{t}_{\text{px}}$. The benefit of the pixel-wise approach is that errors can be localized. Hence, only

suspicious parts of the prediction can be discarded; or warnings can ignored for image regions that are not of interest, such as regions far off the vehicle trajectory in case of a pedestrian detector. A *region-wise monitor* for image regions P marks complete regions or images as spurious based on the pixel truth values. We suggest two definitions derived from M , a simple one and a smoothed one:

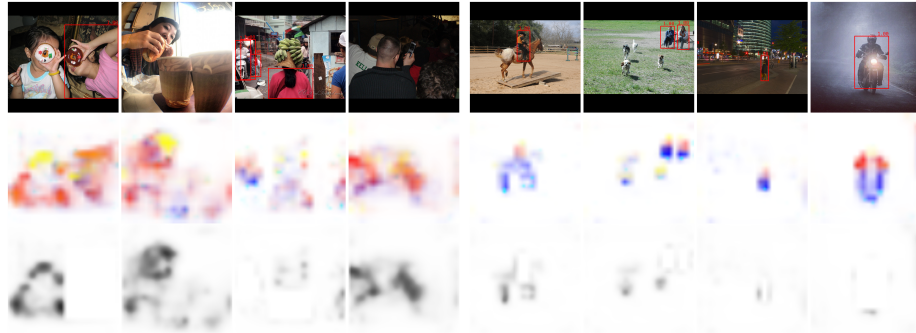
$$M_{\text{reg}}^{\text{simple}}(P) := \exists p \in P: M(p) \stackrel{(*)}{=} \neg R(P) \quad (10)$$

$$M_{\text{reg}}^{\text{peaks}}(P) := \exists p \in P: \text{NbCond}_M(p, P) \stackrel{(**)}{=} \max_{p \in P} \text{AvgPool2D} \left((M(p))_{p \in P} \right) \quad (11)$$

where equality $(*)$ holds if $(\exists x: f(x)) \equiv (\neg \forall x: \neg f(x))$, and equality $(**)$ for $\exists = \max$ and the average pool formulation of NbCond from Eq. (7). The smoothing in Eq. (11) essentially adds a prior on the shape of peaks of monitor pixel values. In general, the choice of quantifier is important: Some are sensitive to outliers, i.e. isolated pixel alarms, and need the smoothing in Eq. (11) (e.g. $\exists = \max$ from Goedel logic), others are sensitive to the ratio between alarm and non-alarm pixels (e.g. mean), or are computationally expensive (e.g. $\exists = \bigvee$ for the probabilistic sum \bigvee from Product logic).

3.2 Concept Analysis for Additional DNN Outputs

Standard object detection outputs usually include only a small set of object classes, e.g. **person**, and no sub-objects or other object attributes allowing for rich semantics. Our goal is to post-hoc enrich the output of a DNN by those concepts that are necessary to formulate given prior domain knowledge like Eq. (1) on DNN inputs and outputs. This should be done (1) without changing the trained DNN, (2) with little additional training and labeling effort, and (3) extensible, i.e. allowing to later add further concepts in case more domain knowledge is collected. For this, supervised post-hoc concept analysis constitutes a suitable candidate. *Concept (embedding) analysis* (CA) in general aims to associate in a simple way semantic concepts with elements in the intermediate output of a DNN, usually that of a layer [31]. Standard types of visual semantic concepts are texture, material, objects, object parts, or image-level concepts like the scene [3]. To achieve the association, supervised CA methods learn to predict information about the concept of interest, e.g. a binary segmentation mask, from the intermediate outputs. We here use the CA method suggested in [31], which was shown to work on CNN object detection. The concept models are attached to the output of one CNN layer. Each consists of a 1×1 -convolution, followed for inference by a sigmoid normalization (and potentially upscaling). This method only introduces minor computational overhead. The output of the concept models are pixel-masks with confidence values in $[0, 1]$, which are trained to match ground truth binary segmentations of the concept. Due to our additional need for well-calibrated outputs (Sec. 3.3), we suggest to exchange the original self-balancing losses from [31] for standard binary cross-entropy loss (BCE) which has less impact on calibration.



Left to right thanks to David Quitoriano, j bizzie, CCFoodTravel.com, k.steudel, Fort Rucker, Donelle, Jacob Bøtter, Vir Nakai; © CC BY 2.0

Fig. 2: EffDet predicted boxes (*top*), concepts (*leg*, *ankle*, *arm*, *wrist*, *eye*; *middle row*), and logical consistency pixel values (*bottom*) for Eq. (11) (before max) with P logic cal setting from Tab. 4. *Left*: Monitor true positives; *right*: false positives.

3.3 Concept Model Calibration

DNN confidence outputs, including our post-hoc attached concept models, may be badly calibrated. This means that the confidence values do not well match the actual probability with which the prediction is correct [9]. When interpreting confidences as fuzzy truth values, bad calibration violates the fundamental assumption that the truth *meaning* monotonously increases with the truth *value*.

Therefore, we suggest to employ approximate Bayesian learning for calibrating our concept models (cf. Sec. 2). We compute a full covariance approximation of the posterior via Laplace approximate [17]. Despite the required Hessian approximation, we still maintain limited computational overhead, as we only apply it to a single layer (cf. Sec. 3.2) with few parameters. This method can be applied without changing or retraining the base model, making it applicable to any pretrained network.

4 Experiments

This section discusses evaluation results for concept model creation (Sec. 4.1) and the three verification use-cases (Sec. 4.2), as well as limitations of our approach (Sec. 4.3). The use-cases are tested on the example occlusion robustness rule from Eq. (1), and for body parts *eye*, *arm*, *wrist*, *leg*, *ankle*. The $\text{Is}_{\text{person}}$ predicate is derived from *person* bounding box outputs of the two networks Mask R-CNN [10] (MR) with ResNet50 backbone, and EfficientDet D1 [33] (EffDet). The weights are trained on the MS COCO train2017 dataset [19], and are taken from PyTorch [27] respectively TensorFlow modelzoo [35] (cf. Tab. 2a for statistics). The ground truth for the body part concepts was derived from the MS COCO 2017 [19] keypoint annotations as done in [31]. Concept models were trained and calibrated on the MS COCO train2017 dataset, with a train/validation split of 4:1. Evaluation results both for the concept model performance and the fuzzy

Table 2: Statistics of used models (2a, 2c) and global consistency scores (2b)

(a) Statistics of used $\text{Is}_{\text{person}}$ predicates				(c) Layer (L) and performance of the used BCE-trained concept models.						
Model	ECE	Pixel-Acc.	sIoU	MR			EffDet			
MR [10]	0.044	0.956	0.810	C	L	sIoU _b	sIoU	L	sIoU _b	sIoU
EffDet [33]	0.071	0.929	0.684	ankle	3	0.210	0.132	4	0.142	0.059
				arm	4	0.330	0.254	6	0.305	0.242
				eye	3	0.436	0.424	5	0.340	0.296
				leg	3	0.326	0.264	5	0.310	0.246
				wrist	4	0.184	0.119	6	0.150	0.069

(b) Global logical consistency scores for rule from Eq. (1)						
	G	G cal	L	L cal	P	P cal
MR	0.994	0.994	0.992	0.991	0.992	0.991
EffDet	0.988	0.985	0.981	0.975	0.982	0.977

Table 3: Calibration and performance of best concept models for MR (statistics averaged over concepts)

	ECE	MCE	sIoU _b	t_{sIoU_b}	sIoU
BCE	0.001 ± 0.000	0.146 ± 0.079	0.297 ± 0.102	0.23 ± 0.06	0.218 ± 0.126
cal	0.001 ± 0.000	0.140 ± 0.082	0.297 ± 0.102	0.24 ± 0.06	0.218 ± 0.126
Dice	0.010 ± 0.008	0.621 ± 0.082	0.265 ± 0.079	0.59 ± 0.20	0.263 ± 0.081
cal	0.001 ± 0.001	0.451 ± 0.121	0.264 ± 0.080	0.52 ± 0.07	0.263 ± 0.080
bBCE	0.083 ± 0.047	0.879 ± 0.037	0.115 ± 0.052	0.95 ± 0.00	0.047 ± 0.031
cal	0.022 ± 0.012	0.772 ± 0.071	0.228 ± 0.054	0.91 ± 0.05	0.056 ± 0.032

logic are collected on the MS COCO val2017 dataset. The performance of $\text{Is}_{\text{person}}$ and the concept model segmentations is evaluated as the set intersection over union (sIoU) [7] between the binary ground truth concept masks $(m_i)_i$ and the predicted and upscaled concept masks $(m_i^{\text{pr}})_i$:

$$\text{sIoU}((m_i)_i, (m_i^{\text{pr}})_i) = \frac{\sum_i \sum m_i \cap (m_i^{\text{pr}} > \text{t}_{\text{sIoU}})}{\sum_i \sum m_i \cup (m_i^{\text{pr}} > 0.5)}. \quad (12)$$

Notation: sIoU_b is measured at optimal t_{sIoU} (determined on a the validation set), sIoU at 0.5.

4.1 Concept Analysis and Calibration

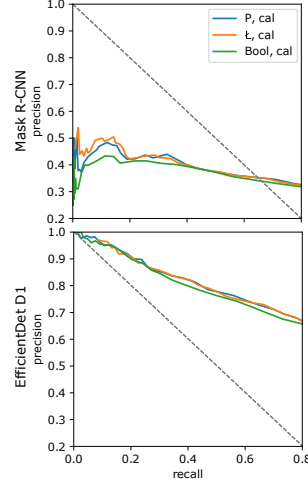
Literature suggests several losses for concept analysis, including balanced Dice loss [31, 28], and a class-balanced binary cross-entropy (bBCE) [7]. We here also consider standard BCE. Tab. 3 compares calibration and performance of these losses in terms of sIoU, expected calibration error (ECE) and maximum calibration error (MCE) [9]. Results show that Laplace-calibrated BCE outperforms all

Table 4: Performance comparison of different formula formulations for image-level monitoring of rule Eq. (1). Metrics: precision-recall (PR) curve, area under ROC curve (AUC), F1 at $t_{\text{reg}}^{\text{peaks}} = 0.5$, and each F1, F0.1, and F10 for the $t_{\text{reg}}^{\text{peaks}}$ yielding the theoretically best corresponding score value.

(a) Image-level results for formula Eq. (1)

		AUC	F1 _{0.5}	F1	F0.1	F10
Mask R-CNN	Bool	0.619	0.146	0.455	0.421	0.975
	Bool cal	0.620	0.144	0.458	0.423	0.975
	L	0.632	0.282	0.462	0.484	0.975
	L cal	0.632	0.295	0.461	0.492	0.975
	P	0.632	0.244	0.466	0.467	0.975
	P cal	0.632	0.243	0.465	0.470	0.975
EfficientDet D1	Bool	0.671	0.421	0.749	0.899	0.993
	Bool cal	0.676	0.411	0.749	0.895	0.993
	L	0.690	0.557	0.752	0.895	0.993
	L cal	0.695	0.592	0.755	0.899	0.993
	P	0.689	0.500	0.751	0.897	0.993
	P cal	0.696	0.523	0.753	0.896	0.993

(b) Upper left part of PR curves



other variants, *given a tuned sIoU threshold*. Interestingly, balanced losses (Dice, bBCE) suffer from substantial miscalibration. This can be partially countered with the Laplace method, but results are still worse. Calibrating the BCE result only shows minor advantages, therefore we re-evaluated the calibration effects for the full approach (cf. Tab. 4). Improvements are still small, but consistent (cf. Sec. 4.2). The sIoU performance of the BCE-trained concept models used in later experiments is given in Tab. 2c. Representations of the larger Mask R-CNN model consistently outperform those of EfficientDet D1 (cf. Sec. 4.2).

4.2 Logical Consistency Monitor Applications

If not stated otherwise (cf. Sec. 4.2), experiments were conducted for the S-implication formulation of the formula from Eq. (1), with trivial CloseBy_σ from Eq. (5), and the arithmetic mean for \forall , and max for \exists (this is $\bigvee_x F(x)$ in Goedel logic). The Goedel exists quantifier was chosen as it is the most conservative one of those defined by fuzzy logics, i.e. yields the smallest values [25, Lemma 2.19]. This is a desirable property for safety evaluation with the example rule. Concept masks are bilinearly upsampled to ensure comparability amongst CNNs. For non-fuzzy logic (Tab. 1), the concept masks are binarized at the same thresholds as the monitor outputs, i.e. $t_{\text{Bool}} = t_{\text{px}}, t_{\text{reg}}$ for $t_{\text{px}}, t_{\text{reg}}$ defined below. A pixel p is a *false negative pixel* ($\text{Is}_{\text{FN}}(p)$), if $\text{Is}_{\text{FN}}(p) \geq t_{\text{ped}} = 0.5$ for $\text{Is}_{\text{FN}}(p) := \neg \text{Is}_{\text{person}}(p) \wedge \text{Is}_{\text{GTPerson}}(p)$. Since the logical consistency monitor Eq. (1) shall highlight false negatives of the detector, Is_{FN} is taken as pixel-wise ground

Table 5: Performance of monitors by binarization threshold \mathbf{t}_{px} , resp. \mathbf{t}_{reg} .(a) Pixel-level ROC AUC
for rule from Eq. (1)

	MR	EffDet
Bool	0.829	0.840
Bool cal	0.830	0.843
L	0.833	0.843
L cal	0.833	0.847
P	0.833	0.843
P cal	0.834	0.847

(b) Prediction-level performance for rule Eq. (13)

		AUC	F1 _{0.5}	$\overline{\text{F1}}$	$\overline{\text{F0.1}}$	$\overline{\text{F10}}$
MR	Bool cal	0.929	0.123	0.230	0.145	0.854
	L cal	0.927	0.136	0.251	0.172	0.844
	P cal	0.930	0.132	0.250	0.172	0.847
EffDet	Bool cal	0.986	0.024	0.118	0.115	0.480
	L cal	0.889	0.028	0.082	0.050	0.464
	P cal	0.985	0.028	0.080	0.048	0.452

truth for the monitor. For evaluation of the pixel-level monitor we binarize the outputs of M (Eq. (9)) at threshold \mathbf{t}_{px} . Note that our formula will only highlight those parts of false negative areas for which the selected body parts were predicted (e.g. not the torso). Hence, pixel-level recall is naturally comparatively low. To investigate suitability for finding images with *some* logical inconsistency, we have a look at the region monitor formulations $M_{\text{reg}}^{\text{simple}}$ (Eq. (10)) and $M_{\text{reg}}^{\text{peaks}}$ (Eq. (11)) for complete images as regions. The ground truth $\mathbf{GT}_{\text{reg}}(P)$ for an image P is defined from the pixel-wise \mathbf{Is}_{FN} values using the same formula as for deriving M_{reg} from M . For evaluation, the predicted and ground truth image scores are binarized using thresholds \mathbf{t}_{reg} respectively $\mathbf{t}_{\text{GTreg}} = 0.5$. The average pooling kernel size \mathbf{ksize} of both $\mathbf{GT}_{\text{reg}}^{\text{peaks}}$ and $M_{\text{reg}}^{\text{peaks}}$ is set to 33 pixels⁵, which approximately coincides with the typical height of a head in the test data (cf. size statistics in [31]) at acceptable memory consumption. This setting means, if half of the pixels within any 33×33 pixels window are false negatives, the image is marked ground truth faulty. In our setting, 27.7% of the test images are marked faulty. For the Bool baseline, \mathbf{t}_{Bool} was set to \mathbf{t}_{px} .

Comparing Monitor Formulations Compared were F1 score, precision, recall and true negative rate of different pixel- (Eq. (9)) and simple image-level (Eq. (10)) monitor formulations at $\mathbf{t}_{\text{px}} = \mathbf{t}_{\text{reg}}^{\text{simple}} = 0.5$. Aspects of variation were: fuzzy logics from Tab. 1; standard R-implication versus strong implication; adding calibration; adding denoising of masks, i.e. setting concept mask values < 0.005 to 0; bilinear upscaling versus maxpool downscaling of concept masks; and the trivial $\mathbf{CloseBy}_{\sigma, r}$ from Eq. (5) versus (only for upscaling) the non-trivial one with $\sigma \approx 2.77$ (truth value of 0.8 at distance of 4px) at $r = 12\text{px}$ (window of $25 \times 25\text{px}$, cutting at truth values below 0.1). Preliminary experiments showed that R-implication produces many false positives at small input truth values, even with denoising. Slight performance improvements were achieved by: fuzziness; calibration for S-implication; the memory-intense $\mathbf{CloseBy}_{\sigma \neq 0}$ on

⁵ Preliminary experiments showed: For $\mathbf{ksize} = 2^i + 1, i \leq 5$, differences between \mathbf{ksize} for \mathbf{GT}_{reg} and M_{reg} only had little influence on the results.

pixel-level; and downscaling for L and P logic, at the cost of truth mask resolution. Therefore, we used the initially described setup for all later experiments.

Self-supervised Error Monitoring Results Compared were Bool, L, and P logic (cf. Tab. 1), each with and without calibration (cal), both for pixel-level (Eq. (9), Tab. 5a) and image-level (Eq. (11), Tab. 4) monitoring. Results show that (1) good error identification performance can be achieved, uncovering a substantial amount of detector errors (cf. [contribution \(v\)](#)); (2) fuzzy evaluations slightly but consistently outperform the non-fuzzy ones and substantially outperform them for precision-biased metrics like $\overline{F0.1}$ score (cf. [contribution \(iii\)](#)); and (3) calibrated slightly outperform non-calibrated versions (cf. [contribution \(iii\)](#)). The image-level results (Tab. 4) further reveal that (4) acceptable precision-recall balances can be achieved for EffDet (e.g. recall of ≥ 0.98 at precision ≥ 0.60 , or precision of ≥ 0.95 at recall ≥ 0.1). This can be seen on the precision-recall curves, as well as from results for F0.1 score (favoring precision) and F10 score (favoring recall) in Tab. 4. Another finding was that (5) the optimal $\tau_{\text{reg}}^{\text{peaks}}$ alarm threshold consistently diverged from the default value 0.5. This suggests that tuning of the threshold on a validation set, similar to τ_{IoU} , may boost performance values. Without tuning, fuzziness brings a considerable benefit (cf. F10.5 in Tab. 4). This is especially of interest for cases when threshold tuning is not viable, e.g., because of tuning data availability or bad generalization of the tuned threshold.

We also considered monitoring of the prediction-level formula for “A person should have a body part” which should reveal false positives of the object detector. With $\text{Is}_{\text{person},i}$ referring to the i th prediction for P :

$$F(P) = (\exists p \in P: \text{Is}_{\text{person},i}(p)) \rightarrow (\exists p \in P: \text{Is}_{\text{person},i}(p) \wedge \text{IsBodyPart}(p)) . \quad (13)$$

A predicted box was defined as false positive (i.e., monitor GT positive) if its person class score was greater 0.5 and it was covered by less than 20 % by the union of GT boxes, producing positive rates of 0.03 % (EffDet) and 1.60 % (MR). Evaluation was conducted using the P logic cal setting from Tab. 4. Here, also, fuzzy approaches outperformed the Boolean one without threshold tuning (Tab. 5b). While performance was low for very small predicted boxes due to the static `ksize` setting and strong class imbalance, it achieved formidable F-scores on larger sized boxes, especially for recall balanced settings which are relevant, e.g. , for sample selection for manual analysis.

Comparing Logical Consistency of Models The better performing and calibrated (cf. Tab. 2a), and ca. three times larger MR model also gives rise to better concept models (Tab. 2c), and achieves higher global logical consistency scores (Tab. 2b). with respect to the the rule from Eq. (1). This aligns with the findings in Tabs. 4 and 5a, where fewer—but still a considerable amount—of the MR false negatives could be recovered using a logical consistency monitor. On the other hand, most errors of the smaller EffDet were recovered using our

simple example rule, attesting the model some simple logical gaps. This promises high potential for improvement of EffDet performance on person detection by fine-tuning towards better logical consistency, or by post-processing based on the monitor outputs.

Corner Case Analysis Finally, we manually inspected the samples with smallest mean pixel-wise logical consistency score for rule Eq. (1)⁶. Here, we exclude pixels p regarded trivial (e.g. background), i.e. such with low alarm score $M(p) \leq 10^{-3}$. See Fig. 2 for example outputs. The analysis revealed for Mask R-CNN: (1) persons segmented by (self-)occlusions may get too small bounding boxes, and (2) person features seem to be confused with that of animals and puppets. And (3) EffDet produces false negatives if the face is only slightly occluded, e.g. by perspective, objects or the image boundary. The found symbolic error modes directly allow to define data augmentation strategies, e.g. adding persons segmented by occlusion. To automate corner case selection from new samples, a threshold τ_{reg} for the logical inconsistency score could be fine-tuned on a validation set. Altogether, the fuzzy rule evaluation helps in finding semantic error modes.

4.3 Limitations

Result quality depends on that of the framework ingredients: the concept models and the rules. Bad convergence, a bias in the concept samples, or simply insufficient CNN representations may lead to erroneous concept masks. And the prior knowledge rules are naturally susceptible to human bias (e.g. anatomical assumptions), potentially leading to unfair safety guarantees. Besides that, inconsistencies with those pre-defined rules are not guaranteed to accurately correspond to errors. Our approach potentially considerably reduces the amount of test data needed to uncover issues and it enables self-supervision, but, thus, naturally inherits all limitations of data based verification methods, like test data representativity. And lastly, parts of our simple initial modeling approach may be improved. This concerns the simplistic CNN output transformation, GT definition, and the neighborhood condition from Eq. (7) which currently does not take into account object sizes, so still cannot prevent all occurrences of “over-shooting”.

5 Conclusion and Outlook

This work presents a simple, yet flexible, post-hoc, self-supervised method to verify and monitor outputs of trained CNNs regarding compliance with symbolic domain knowledge rules. It is the first that requires no architectural constraints or changes to already trained CNNs, and permits later extension of the rule base.

⁶ Precisely, images P_{img} with highest $M_{\text{reg}}^{\text{simple}}(P)$ value from Eq. (10) for the region $P = \{p \in P_{\text{img}} \mid M(p) \geq 10^{-3}\} \subset P_{\text{img}}$.

The method comes with little computational overhead, and allows to leverage fuzziness and calibration for slight performance benefits. We showed how to use it to identify a considerable proportion of detection errors. Furthermore, the used logical consistency scores can help in finding error modes, and to directly compare CNNs. For example, in comparison to EfficientDet D1, Mask R-CNN shows considerably better representations and conformity with a simple occlusion robustness rule for person detection.

We are looking forward to see results on further models, tasks, and example rules, including investigation of how to model temporal aspects, and how to advance our initial modeling suggestions. Also, it seems promising to study how much a trained model could be improved by self-supervised fine-tuning via the logical consistency scores.

Acknowledgments

The research leading to these results is partly funded by the German Federal Ministry for Economic Affairs and Energy within the project “KI Absicherung – Safe AI for Automated Driving”. The authors would like to thank the consortium for the successful cooperation.

References

1. Abdar, M., Pourpanah, F., Hussain, S., Rezazadegan, D., Liu, L., Ghavamzadeh, M., Fieguth, P., Cao, X., Khosravi, A., Acharya, U.R., Makarenkov, V., Nahavandi, S.: A review of uncertainty quantification in deep learning: Techniques, applications and challenges. *Information Fusion* **76**, 243–297 (2021). <https://doi.org/https://doi.org/10.1016/j.inffus.2021.05.008> **3**
2. Badreddine, S., d’Avila Garcez, A., Serafini, L., Spranger, M.: Logic tensor networks. *CoRR* **abs/2012.13635** (Jan 2021), <https://arxiv.org/abs/2012.13635> **3**, **5**
3. Bau, D., Zhou, B., Khosla, A., Oliva, A., Torralba, A.: Network dissection: Quantifying interpretability of deep visual representations. In: *Proc. 2017 IEEE Conf. Comput. Vision and Pattern Recognition*. pp. 3319–3327. IEEE Computer Society (2017). <https://doi.org/10.1109/CVPR.2017.354> **2**, **8**
4. Cheng, C.H., Nührenberg, G., Huang, C.H., Ruess, H., Yasuoka, H.: Towards dependability metrics for neural networks. In: *16th ACM/IEEE Int. Conf. Formal Methods and Models for System Design*. pp. 43–46. IEEE (2018). <https://doi.org/10.1109/MEMCOD.2018.8556962> **3**
5. Diligenti, M., Gori, M., Saccà, C.: Semantic-based regularization for learning and inference. *Artificial Intelligence* **244**, 143–165 (Mar 2017). <https://doi.org/10.1016/j.artint.2015.08.011> **3**
6. Donadello, I., Serafini, L., d’Avila Garcez, A.S.: Logic tensor networks for semantic image interpretation. In: *Proc. 26th Int. Joint Conf. Artificial Intelligence*. pp. 1596–1602. *ijcai.org* (2017). <https://doi.org/10.24963/ijcai.2017/221> **2**, **5**, **22**, **23**
7. Fong, R., Vedaldi, A.: Net2Vec: Quantifying and explaining how concepts are encoded by filters in deep neural networks. In: *Proc. 2018 IEEE Conf. Comput. Vision and Pattern Recognition*. pp. 8730–8738. IEEE Computer Society (2018). <https://doi.org/10.1109/CVPR.2018.00910> **2**, **3**, **10**

8. Fong, R.C., Vedaldi, A.: Interpretable explanations of black boxes by meaningful perturbation. In: Proc. 2017 IEEE Int. Conf. on Comput. Vision. pp. 3449–3457. IEEE Computer Society (2017). <https://doi.org/10.1109/ICCV.2017.371> 3
9. Guo, C., Pleiss, G., Sun, Y., Weinberger, K.Q.: On calibration of modern neural networks. In: Precup, D., Teh, Y.W. (eds.) Proceedings of the 34th International Conference on Machine Learning, ICML 2017, Sydney, NSW, Australia, 6–11 August 2017. Proceedings of Machine Learning Research, vol. 70, pp. 1321–1330. PMLR (2017), <http://proceedings.mlr.press/v70/guo17a.html> 3, 9, 10
10. He, K., Gkioxari, G., Dollár, P., Girshick, R.: Mask R-CNN. In: 2017 IEEE International Conference on Computer Vision (ICCV). pp. 2980–2988 (Oct 2017). <https://doi.org/10.1109/ICCV.2017.322> 9, 10
11. Hüllermeier, E.: Does machine learning need fuzzy logic? Fuzzy Sets and Systems **281**, 292–299 (Dec 2015). <https://doi.org/10.1016/j.fss.2015.09.001> 2
12. Kazhdan, D., Dimanov, B., Terre, H.A., Jamnik, M., Liò, P., Weller, A.: Is disentanglement all you need? comparing concept-based & disentanglement approaches. arXiv:2104.06917 [cs] (Apr 2021), <http://arxiv.org/abs/2104.06917> 2
13. Kim, B., Wattenberg, M., Gilmer, J., Cai, C., Wexler, J., Viegas, F., Sayres, R.: Interpretability beyond feature attribution: Quantitative testing with concept activation vectors (TCAV). In: Proc. 35th Int. Conf. Machine Learning. Proceedings of Machine Learning Research, vol. 80, pp. 2668–2677. PMLR (Jul 2018), <http://proceedings.mlr.press/v80/kim18d.html> 2, 3
14. Kingma, D.P., Ba, J.: Adam: A method for stochastic optimization. In: Proc. 3rd Int. Conf. Learning Representations (2015), <http://arxiv.org/abs/1412.6980> 20
15. Kingma, D.P., Salimans, T., Welling, M.: Variational dropout and the local reparameterization trick. In: Cortes, C., Lawrence, N., Lee, D., Sugiyama, M., Garnett, R. (eds.) Advances in Neural Information Processing Systems. vol. 28. Curran Associates, Inc. (2015), <https://proceedings.neurips.cc/paper/2015/file/bc7316929fe1545bf0b98d114ee3ecb8-Paper.pdf> 3
16. Krishnan, R., Tickoo, O.: Improving model calibration with accuracy versus uncertainty optimization. In: Advances in Neural Information Processing Systems 33: Annual Conference on Neural Information Processing Systems 2020, NeurIPS 2020, December 6–12, 2020, virtual (2020), <https://proceedings.neurips.cc/paper/2020/hash/d3d9446802a44259755d38e6d163e820-Abstract.html> 3
17. Kristiadi, A., Hein, M., Hennig, P.: Being bayesian, even just a bit, fixes overconfidence in relu networks. In: Proceedings of the 37th International Conference on Machine Learning, ICML 2020, 13–18 July 2020, Virtual Event. Proceedings of Machine Learning Research, vol. 119, pp. 5436–5446. PMLR (2020), <http://proceedings.mlr.press/v119/kristiadi20a.html> 3, 9
18. Lapuschkin, S., Wäldchen, S., Binder, A., Montavon, G., Samek, W., Müller, K.R.: Unmasking Clever Hans predictors and assessing what machines really learn. Nature Communications **10**(1), 1096 (Mar 2019). <https://doi.org/10.1038/s41467-019-08987-4> 3
19. Lin, T.Y., Maire, M., Belongie, S.J., Hays, J., Perona, P., Ramanan, D., Dollár, P., Zitnick, C.L.: Microsoft COCO: Common objects in context. In: Proc. 13th European Conf. Computer Vision - Part V. Lecture Notes in Computer Science, vol. 8693, pp. 740–755. Springer International Publishing (2014). https://doi.org/10.1007/978-3-319-10602-1_48 9, 20
20. Liu, C., Arnon, T., Lazarus, C., Strong, C., Barrett, C., Kochenderfer, M.J.: Algorithms for verifying deep neural networks. Foundations and Trends® in Optimization **4**(3–4), 244–404 (Feb 2021). <https://doi.org/10.1561/24000000035> 2

21. Liu, L., Ouyang, W., Wang, X., Fieguth, P., Chen, J., Liu, X., Pietikäinen, M.: Deep learning for generic object detection: A survey. *International Journal of Computer Vision* **128**(2), 261–318 (Feb 2020). <https://doi.org/10.1007/s11263-019-01247-4> 2
22. MacKay, D.J.C.: The evidence framework applied to classification networks. *Neural Comput.* **4**(5), 720–736 (1992). <https://doi.org/10.1162/neco.1992.4.5.720> 20, 21
23. Marra, G., Giannini, F., Diligenti, M., Gori, M.: LYRICS: A general interface layer to integrate logic inference and deep learning. In: *Proc. European Conf. Machine Learning and Principles of Knowledge Discovery 2019* (Sep 2019), <http://arxiv.org/abs/1903.07534> 3
24. Nandwani, Y., Pathak, A., Mausam, Singla, P.: A primal dual formulation for deep learning with constraints. In: *Advances in Neural Information Processing Systems* 32. pp. 12157–12168. Curran Associates, Inc. (2019), <http://papers.nips.cc/paper/9385-a-primal-dual-formulation-for-deep-learning-with-constraints.pdf> 3
25. Novák, V., Perfilieva, I., Mockor, J.: *Mathematical Principles of Fuzzy Logic*. The Springer International Series in Engineering and Computer Science, Springer US (Jan 1999). <https://doi.org/10.1007/978-1-4615-5217-8> 1, 2, 3, 4, 5, 11
26. Perello-Nieto, M., Filho, T.D.M.E.S., Kull, M., Flach, P.: Background check: A general technique to build more reliable and versatile classifiers. In: *2016 IEEE 16th International Conference on Data Mining (ICDM)*. pp. 1143–1148. IEEE (Dec 2016). <https://doi.org/10.1109/ICDM.2016.0150> 3
27. pytorch: Torchvision (Oct 2021), <https://github.com/pytorch/vision/v0.10.0> 9
28. Rabold, J., Schwalbe, G., Schmid, U.: Expressive explanations of DNNs by combining concept analysis with ILP. In: *KI 2020: Advances in Artificial Intelligence*. pp. 148–162. *Lecture Notes in Computer Science*, Springer International Publishing (2020). https://doi.org/10.1007/978-3-030-58285-2_11 10
29. Rottmann, M., Colling, P., Paul Hack, T., Chan, R., Hüger, F., Schlicht, P., Gottschalk, H.: Prediction error meta classification in semantic segmentation: Detection via aggregated dispersion measures of softmax probabilities. In: *Proc. 2020 Int. Joint Conf. Neural Networks*. pp. 1–9 (Jul 2020). <https://doi.org/10.1109/IJCNN48605.2020.9206659> 3
30. Roychowdhury, S., Diligenti, M., Gori, M.: Image classification using deep learning and prior knowledge. In: *Workshops of the 32nd AAAI Conf. Artificial Intelligence*. AAAI Workshops, vol. WS-18, pp. 336–343. AAAI Press (Jun 2018), <https://aaai.org/ocs/index.php/WS/AAAIW18/paper/view/16575> 3
31. Schwalbe, G.: Verification of size invariance in DNN activations using concept embeddings. In: *Artificial Intelligence Applications and Innovations*. pp. 374–386. *IFIP Advances in Information and Communication Technology*, Springer International Publishing (2021). https://doi.org/10.1007/978-3-030-79150-6_30 2, 3, 6, 8, 9, 10, 12, 20
32. Schwalbe, G., Schels, M.: A survey on methods for the safety assurance of machine learning based systems. In: *Proc. 10th European Congress Embedded Real Time Software and Systems* (Jan 2020), <https://hal.archives-ouvertes.fr/hal-02442819> 1
33. Tan, M., Pang, R., Le, Q.V.: EfficientDet: Scalable and efficient object detection. In: *Proc. 2020 IEEE/CVF Conf. Comput. Vision and Pattern Recognition*. pp. 10781–10790 (2020) 9, 10

34. Wang, D., Cui, X., Wang, Z.J.: CHAIN: Concept-harmonized hierarchical inference interpretation of deep convolutional neural networks. CoRR **abs/2002.01660** (2020), <https://arxiv.org/abs/2002.01660> 3
35. Wightman, R.: EfficientDet (PyTorch) (Oct 2021), <https://github.com/rwightman/efficientdet-pytorch/tree/75e16c2f> 9

Appendix Overview

This supplemental material collects additional results and details for the experiments described in the main paper. Specifically, it gives further evidence for the following claims made in the main paper:

- Appendix B: *The main formula for false negative detection used in the main paper can be implemented as parallelizable windowed operation* under some modeling constraints.
- Appendix C: This section gives detailed results of the preliminary experiments on the comparison of monitor formulations referenced in the main paper. These show that *the simple rule formulation used in the main paper is a valid choice* for the later experiments in the main paper.
- Appendix D: *Fuzziness improves the error-detection performance of a logical consistency monitor when the hyperparameter for the binarization threshold cannot be tuned* on a validation set.
- Appendix E: For the peak-concentrated image-level monitor formulation, *the kernel size hyperparameter of the monitor can be chosen independently of that of the ground truth*.

Appendix A gives details on the chosen hyperparameter values for the experiments to ensure reducibility.

Table 6: Overview of hyperparameters and their default values used in the formula calculation (here and in the main paper).

Name	Default	Function
t_{sIoU}	0.5	Threshold used to determine the set intersection over union performance
$t_{denoise}$	0.005	Denoise low values of $Is_{BodyPart}(\bullet)$ masks
t_{ped}	0.5	Binarizing threshold for $Is_{person}(\bullet)$ masks
t_{px}	0.5	Binarizing threshold for pixel-level monitor output masks
t_{reg}	0.5	Binarizing threshold for image-level monitor outputs
t_{sIoU}	0.5	Binarizing threshold for pixel-level monitor outputs for measuring sIoU
t_{Bool}	0.5	Binarizing threshold for all mask in non-fuzzy logic
$ksize$	33	Width of the quadratic kernel for defining a (binary) pixel neighborhood

A Implementation Notes: Hyperparameter Choices

In the following, hyperparameter choices for our experiments are detailed. An overview on further hyperparameters introduced in this supplemental material and the main paper can be found in Tab. 6.

Settings applicable to all experiments are:

- An image size of 400×400 pixels was used for Mask R-CNN, 640×640 pixels for EfficientDet D1.
- Images were first zero-padded to square size, then resized to the desired image size (keeping the aspect ratio).
- For metrics working on binary pixel values, output masks (after transformation of bounding boxes to masks) are thresholded at a value of 0.5.

Concept Data The body part segmentation masks were generated from keypoint annotations as proposed in [31]. Point concepts (eye, wrist, ankle) are added as filled circle of white pixels. Limb concepts (arm, leg) get filled circles at edges and joints, and lines connecting them where skeletal connections exist. The concepts consist of the following keypoints:

- arm: left/right shoulder, elbow, wrist
- leg: left/right hip, knee, ankle
- eye, wrist, ankle: corresponding left/right keypoints

Circle diameter and line width were set to 5% of the estimated person body height in pixels (using estimation algorithm from [31]). The body height defaults to the bounding box height if it cannot be estimated from keypoint links of the annotation. Keypoints annotated as occluded are treated as not present.

Calibration and Formula Evaluations The measurement of calibration and performance metrics on the main CNN, as well as the evaluations of the fuzzy logic formulas, used the following settings:

- Evaluation batch size: 64;
- Data split: All images from the MS COCO dataset [19] val2017 split are used for evaluation.

Concept Model Training The training and evaluation of the concept models used the following settings in accordance with [31]:

- Metric and loss calculation: Concept model outputs (after convolution) are first bilinearly upsampled to match the ground truth resolution, then normalized. For BCE-losses, normalization is skipped and the loss is calculated in logit space.
- Loss for second stage training of the Laplace approximation parameters [22]: binary cross-entropy (in logit space);
- Data split: The training and validation data sets are taken from the MS COCO dataset [19] train2017 split, the test data from the val2017 split. For each concept, only those samples are included that contain any positive concept mask pixel. The train2017 samples for a concept are randomly split into training and validation set, at a ratio of 4:1.
- Optimizer and learning rate: Adam [14] from PyTorch version 1.9.0 implementation, with a learning rate of 0.001, and default beta values of 0.9 and 0.999; no weight decay;

- Batch sizes: 8 for training, 64 for validation, and 6 for the second stage training of the Laplace approximation parameters [22];
- Early stopping: Concept models are trained for at most 7 epochs. Training is stopped early after an epoch if the validation loss decreases less than 0.001 for each in three successive epochs.

B Implementation Notes: Parallelization of Example Formula

Consider the mask operation CloseToA_b that accepts a mask Q and returns a mask P with each pixel p holding the truth value for “ p is close to a pixel q in Q at which concept b is present”. This is used in the example formula from the main paper as will become clear from Def. 2. This section shows that under some conditions this CloseToA_b **can be implemented as a windowed operation** on the mask Q , similar to a convolution or pooling operation. Furthermore, an upper bound is given for the minimal window size (cf. Prop. 1). The **windowing allows parallelization, and thus a potentially massive speedup**. Note, however, that this may be quite memory intensive, as it is not guaranteed that the operation can be represented as sparse matrix operations.

Before formally defining CloseToA_b in Def. 2, some notation for pixel indices is introduced that allows to interpret them as coordinates (with standard distance measures like L_1).

Definition 1. Let h, h', w, w' be natural numbers (mask heights and widths), and let $Q \in [0, 1]^{h' \times w'}$, $P \in [0, 1]^{h \times w}$ be 2D masks. A mask coordinate system here denotes an injective mapping of dimensions (i_h, i_w) in a mask P to pixel positions in 2D space \mathbb{R}^2 . By default map the dimension (i_h, i_w) to the point $(i_h + 0.5, i_w + 0.5)$, i.e. a pixel has a width of 1×1 and pixel coordinates refer to pixel centers. Let $p \in \mathbb{R}^2$ be a pixel position.

- (a) *Pixel positions in a mask:* Denote by $p \in P$ that p is a pixel in the mask P .
- (b) *Pixel values of a mask:* Given that $p \in P$, denote by $P(p)$ the value at the pixel position p in the mask P .
- (c) *Sub-masks of a mask:* A mask $W \in [0, 1]^{h \times w}$ is a window or sub-mask in $P \in [0, 1]^{h' \times w'}$, denoted $W \subset P$, if $h \leq h', w \leq w'$, and there is a mask coordinate system for W and P such that for all pixel positions $p \in W$ holds $p \in P$ and $W(p) = P(p)$.

Definition 2. Let h, h', w, w' be integers and $Q \in [0, 1]^{h' \times w'}$ be a mask. Assume a logic is given with predicates Is_b and CloseBy of arity one respectively two, which both operate on pixel positions. We define the following mask operation:

$$\text{CloseToA}_b: [0, 1]^{h' \times w'} \rightarrow [0, 1]^{h \times w} \quad (14)$$

$$P(p) := (\exists q \in Q: \text{Is}_b(q) \wedge \text{CloseBy}(p, q)) \quad (15)$$

for $p \in P := \text{CloseToA}_b(Q)$.

This is used in the example formula from the main paper. (Note that P and Q need not have the same resolution.)

The following proposition states that, under some conditions, CloseToA_b can be implemented as a windowed operation. And, if the CloseBy predicate becomes zero at some L_1 distance r , the window size of the windowed operation may be chosen $2r + 1$ (or smaller). This means, $2r + 1$ is the maximum window size necessary to ensure an exact implementation.

Proposition 1. *Consider a (fuzzy) logic, and Is_b , CloseBy , and the masks Q and $P = \text{CloseToA}_b(Q)$ as in Def. 2. Assume the following:*

- (a) \exists is either defined as an arithmetic mean [6], or defined using the logical OR, i.e. for a domain X and a formula f holds $\exists x \in X: f(x) := \bigvee_{x \in X} f(x)$.
- (b) There is a square integer window size $2r + 1$ such that $\text{CloseBy}(p, q) = 0$ if $\|p - q\|_1 > r$ for any pixel positions p, q . This is e.g. the case for the suggested maxpooling or Gaussian CloseBy from the main paper.

Then, $P(p)$ for a pixel position $p \in P$ at most depends on the pixel values in the window $W_p \subset Q$ of size $(2r + 1) \times (2r + 1)$ centered at p , i.e.

$$\text{CloseToA}_b(Q)(p) = (\exists q \in W_p: Is_b(q) \wedge \text{CloseBy}(p, q)) \quad (16)$$

Proof. Let $f(p, q) := Is_b(q) \wedge \text{CloseBy}(p, q)$. Note that

- (i) $f(p, q) = 0$ if $\text{CloseBy}(p, q) = 0$, and
- (ii) $q \in W_p$ if $f(p, q) \neq 0$, because for $q \in Q \setminus W_p$ holds:
 - $\|p - q\|_1 > r$ by definition of the window W_p , thus
 - $\text{CloseBy}(p, q) = 0$ by (b), and so
 - $f(p, q) = 0$ by (*).

For \exists defined via logical OR according to assumption (a), the formula becomes

$$P(p) = \exists q \in Q: f(p, q) \stackrel{(a)}{=} \bigvee_{q \in Q} f(p, q) \quad (17)$$

$$\stackrel{(i)}{=} 0 \vee \bigvee_{\substack{q \in Q \\ f(p, q) \neq 0}} f(p, q) \stackrel{(ii)}{=} 0 \vee \bigvee_{\substack{q \in W_p \\ f(p, q) \neq 0}} f(p, q) \quad (18)$$

$$\stackrel{(a)}{=} \exists q \in W_p: f(p, q) \quad (19)$$

For \exists defined via arithmetic mean, note that

$$\exists q \in Q: f(p, q) = \frac{1}{\#Q} \sum_{q \in Q} f(p, q). \quad (20)$$

Replacing all occurrences of $\bigvee_{q \in Q}$ with $\frac{1}{\#Q} \sum_{q \in Q}$ in the above calculation finalizes the proof.

Remark 1. Note that the notation, Def. 2, and Prop. 1 all can easily be generalized to masks $Q \in [0, 1]^{n_1 \times \dots \times n_d}$ of arbitrary dimension $d \geq 1$, with pixel positions in \mathbb{R}^d . So, the rule formulation and efficient implementation can be applied not only to 2D masks, but also e.g. 3D masks consisting of several channels or frames.

Remark 2. The following special cases further simplify the implementation:

- (a) *Trivial case:* In case $r = 1$, as in the experiments in the main paper, $\text{CloseToA}_b(Q)(p) = \text{Is}_b(p) \wedge \text{CloseBy}(p, p)$.
- (b) *Maxpooling case:* For $\exists = \max$ and binary

$$\text{CloseBy}(p, q) := (\|p - q\|_1 \leq r) \quad (21)$$

($\text{CloseBy}(p, q)$ is one if q lies in a square window around p , else 0) CloseToA_b becomes a simple maxpooling operation on Q with kernel size $2r + 1$. The stride of the pooling operation is such that the size $h' \times w'$ of Q is reduced to the size $h \times w$ of P . This is used for the downscaling operation which was suggested in the main paper and is further investigated in Appendix C.

- (c) *Convolutional case:* For $\exists = \text{mean}$ [6] and Product logic, CloseToA_b becomes a simple linear convolution followed by applying a pixel-wise factor $\frac{1}{(h' \cdot w')^2}$. Kernel weights for the kernel window with center p are defined by $\text{CloseBy}(p, \cdot)$.

C Comparison of Monitor Formulations

This section collects further considerations and the results for directly comparing different monitor formulations. The following variations are considered (cf. Tab. 7):

Fuzzy logics from the main paper: Łukasiewicz, Product, and Goedel fuzzy logic; and non-fuzzy predicate logic on concept masks binarized at \mathbf{t}_{Bool} .

Implication style: Strong implication (S-implies) or residuated implication (R-implies).

Denoising: With or without setting concept mask values lower than $\mathbf{t}_{\text{denoise}} = 0.005$ to 0. This can be modeled as pixel-wise operation $(\text{Is}_b(p) \geq \mathbf{t}_{\text{denoise}}) \wedge \text{Is}_b(p)$ for pixels p and concept b with concept mask $\text{Is}_b(\cdot)$.

Choice of CloseBy: Considered are the Gaussian $\text{CloseBy}_{\sigma, r}$ from the main paper, different mask scaling options, and trivial $\text{CloseBy}_{\sigma=0, r=1}$. The following three settings are compared here:

- bilinear upscaling with trivial CloseBy
- bilinear upscaling with non-trivial $\text{CloseBy}_{\sigma, r}$, $\sigma \approx 2.77$ and $r = 12\text{px}$ (*in visualizations shorted to CoveredBy*)
- downscaling using maxpooling with trivial CloseBy

Calibration: With or without post-hoc Laplace calibration of concept model outputs.

On the Denoising The *denoising* intends to reduce the instable cases of pixels for R-implies. These are the cases where both values of `IsBodyPart` and `Isperson` are very low, but `IsBodyPart` is larger than `Isperson`. For Product and Goedel logic this causes $\text{IsBodyPart}(p) \rightarrow_R \text{Is}_{\text{person}}(p)$ to jump from 1 to a smaller value (cf. R-implies definitions from the main paper).

On the CloseBy Choice Either approach for *implementing CloseBy*—the fuzzy but memory-intense Gaussian `CloseBy σ, r` , and the non-fuzzy maxpooling based one—has the effect of enlarging the area of positive truth values. This is useful if concept masks have different resolutions and might not match precisely at the boundaries. This leads to low truth values in boundary regions if a low-resolution mask and a higher-resolution mask are scaled and combined in a *AND* or *implies* operation.

Results Results for the following monitor formulations can be found below (both using binarization thresholds $\tau_{\text{px}} = 0.5 = \tau_{\text{reg}}^{\text{simple}}$):

- Pixel-wise monitor M : Fig. 3 for Mask R-CNN, Fig. 4 for EfficientDet D1.
- Image-level monitor $M_{\text{reg}}^{\text{simple}}$: Fig. 5 for Mask R-CNN, Fig. 6 for Efficient-Det D1.

Furthermore, global scores for different monitor formulations are compared in Fig. 7. It must be noted that the pixel-level monitor is expected to have low recall: Only such detector false negative pixels should be highlighted that are inconsistent with the considered rule, which can only be those that are part of one of the considered body parts (no torso, bounding box corners, etc.). The following can be seen from the visualizations:

- (1) *Fuzziness*: For S-implication, **non-fuzzy logic performs consistently slightly worse than fuzzy logic.**
- (2) *Implication style and denoising*: Despite denoising, **R-implication is still much too sensitive** and causes many false positives (cf. low true negative rates, and suspiciously high recall on pixel-level).
- (3) *CloseBy*: **Using a non-trivial CloseBy gives slight (downscaling) up to significant (non-trivial CloseBy _{σ, r}) performance benefits**, as can be seen e.g. from the F1 scores. However, `CloseBy σ, r` either cannot be parallelized or requires lots of memory for the windowed operation, and downscaling significantly reduces (localization) information. Thus, in the main paper only the trivial `CloseBy` is used, and noise problems smoothed using the neighborhood condition for the image-level monitor (cf. Appendix E).
- (4) *Calibration* on pixel-level seems to have a **negative effect on precision and a positive one on recall, resulting in comparable F1 scores.** On image-level, calibration seems to have the least effect of all aspects of variation on the monitor performance. **For the global scores calibration has the visible effect of decreasing logical consistency for any rule formulation.**

- (5) The comparison of the lack of *global logical consistency* in Fig. 7 shows that **the choice of rule formulation has no influence on the trend of the global consistency**. Any choice of variation attests EfficientDet D1 the clearly worse score.

Table 7: Overview on the different aspects of variation tested for the formulation of the formula from the main paper (cf. Appendix C)

Aspect	Description
Implication	Whether S- or R-implication is used
closeBy, Scaling	Formulation of the closeBy: upscaling of small masks with either non- or trivial closeBy _{σ, r} ; or max-downscaling of large masks
Calibration	Whether Laplace calibration is applied to the concept models during inference
Denoising	Whether truth values in concept masks $\mathbf{I}_{\mathbf{s}_b}(\cdot)$ that are below $\mathbf{t}_{\text{denoise}}$ are set to 0

D Benefits of Fuzziness without Monitor Threshold Tuning

Fig. 8 shows the F1 scores of the pixel- and the image-level monitors considered in the main paper, plotted by the binarization threshold \mathbf{t}_{px} respectively $\mathbf{t}_{\text{reg}}^{\text{peaks}}$. Concretely compared are the non-fuzzy baseline with Łukasiewicz and Product t-norm fuzzy logic, with calibrated and non-calibrated concept models. The following can be seen:

- (1) **When deviating from the optimal threshold, fuzzy formulations clearly outperform the non-fuzzy alternative.**
- (2) The optimal thresholds, and corresponding optimal $\overline{\text{F1}}$ scores on the test set nearly coincide for all formulations.
- (3) In all cases, F1-by-threshold curve has a unique maximum, and the threshold for this optimal F1 score is far from the default of 0.5. This **highlights the potential performance increase by tuning the hyperparameter \mathbf{t}_{px} respectively $\mathbf{t}_{\text{reg}}^{\text{peaks}}$.**
- (4) It can be seen a consistent slight performance benefit of calibration.

E Choice of ksize for Image-level Monitor

The peak-concentrated image-level monitor $M_{\text{reg}}^{\text{peaks}}$ used in experiments in the main paper has the additional hyperparameter of the average pooling kernel size **ksize** for the image-level monitor neighborhood condition. As both the monitor $M_{\text{reg}}^{\text{peaks}}$ and $\text{GT}_{\text{reg}}^{\text{peaks}}$ were defined using the neighborhood condition, each has a tunable **ksize** parameter, **ksize_M** and **ksize_{GT}**.

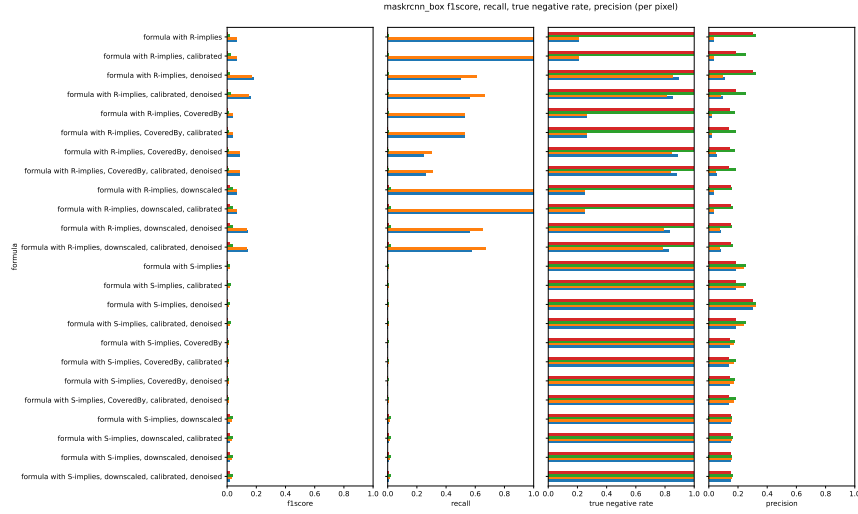


Fig. 3: **Mask R-CNN, pixel-level monitor**: Visual comparison of performance metrics for different monitor formulations (cf. Tab. 7). *Left to right*: F1 score, recall, precision, and true negative rate.

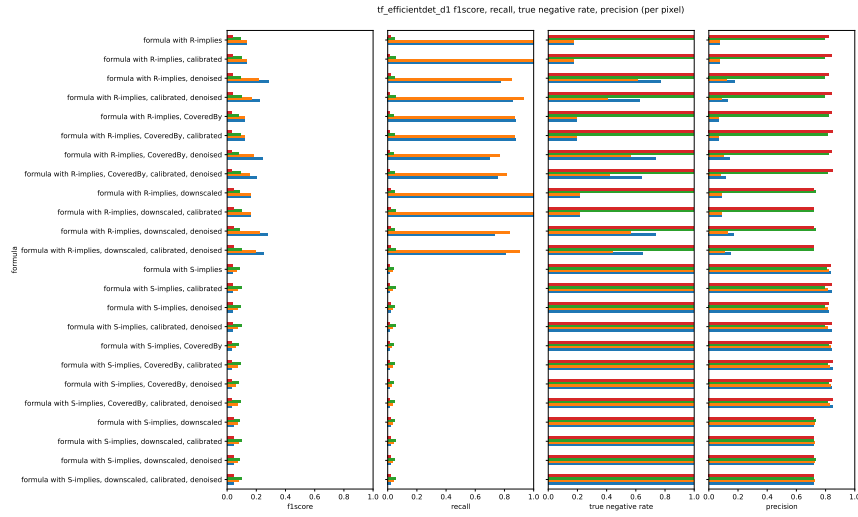


Fig. 4: **EfficientDet D1, pixel-level monitor**: Visual comparison of performance metrics for different monitor formulations (cf. Tab. 7). *Left to right*: F1 score, recall, precision, and true negative rate.

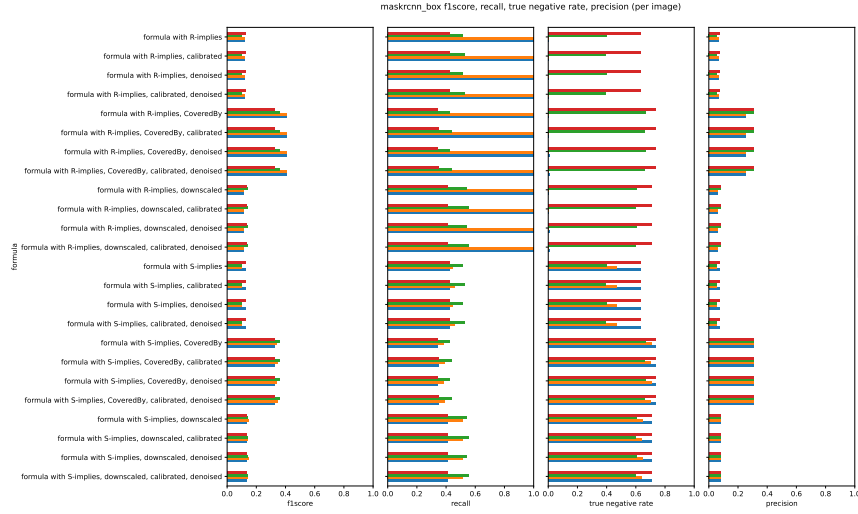


Fig. 5: **Mask R-CNN**, **image-level** monitor: Visual comparison of performance metrics for different monitor formulations (cf. Tab. 7). *Left to right*: F1 score, recall, precision, and true negative rate.

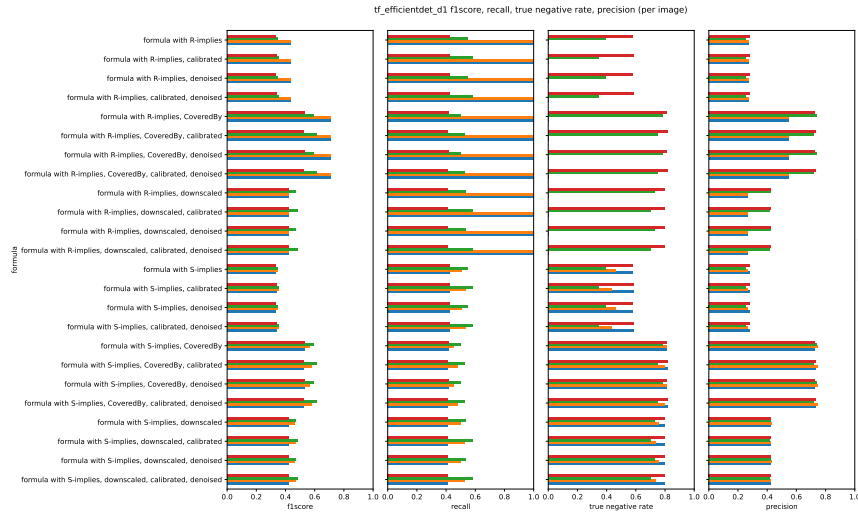


Fig. 6: **EfficientDet D1**, **image-level** monitor: Visual comparison of performance metrics for different monitor formulations (cf. Tab. 7). *Left to right*: F1 score, recall, precision, and true negative rate.

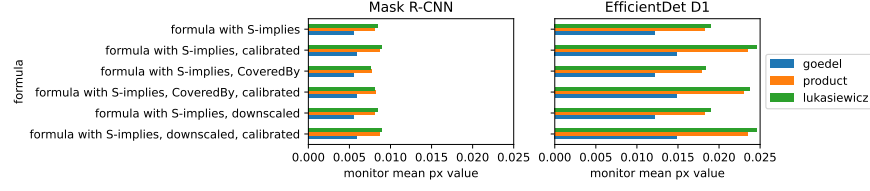


Fig. 7: Comparison of values of $(1 - \text{global score})$ for different monitor formulations. This calculates as the mean of the pixel-wise monitor values over the complete dataset.

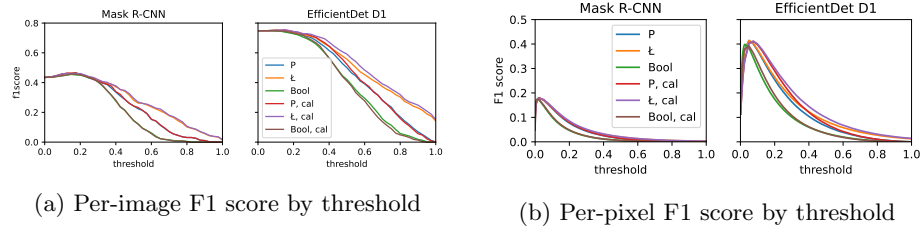


Fig. 8: F1 score by $\mathbf{t}_{\text{reg}}^{\text{peaks}}$ (image-level, Fig. 8a) and \mathbf{t}_{px} (pixel-level, Fig. 8b) for the versions of the simple rule formulations compared in the main paper.

Ground Truth Positive Rates $\mathbf{ksize}_{\text{GT}}$ influences the ground truth positive rate of images in the dataset, as smaller kernel window size values are more sensible to smaller (possibly noisy) peaks. Tab. 8 shows the positive rates for exponentially increasing $\mathbf{ksize}_{\text{GT}}$ and two $\mathbf{t}_{\text{GTreg}}^{\text{peaks}}$ settings. What positive rate is obtained for which \mathbf{ksize} setting depends on the distribution of alarm area sizes in the test dataset. For example, for $\mathbf{t}_{\text{GTreg}}^{\text{peaks}}$ the positive rate approximately linearly increases with the kernel size. Note that for $\mathbf{ksize}_{\text{GT}}$, this is identical with the ground truth for the simple monitor formulation $M_{\text{reg}}^{\text{simple}}$.

Dependence of Monitor Results on $\mathbf{ksize}_{\text{GT}}$ The following results show that larger kernel sizes of the monitor (prediction) bring some benefit, regardless of the ground truth kernel size. Investigated were odd kernel sizes $2^i + 1$, $2 \leq i \leq 5$ and kernel size of 1 as baseline. Here evaluated were the neighborhood (nb) image-level formulation of the monitor from the main paper, for the rule formulation with S-implication and calibration. Compared were different Łukasiewicz and non-fuzzy logic, different kernel sizes $\mathbf{ksize}_M, \mathbf{ksize}_{\text{GT}}$, and binarization thresholds $\mathbf{t}_{\text{reg}}^{\text{peaks}}, \mathbf{t}_{\text{GTreg}}^{\text{peaks}}$. Results are shown

- for fixed middle sized $\mathbf{ksize}_{\text{GT}} = 9$ in Fig. 9,
- for \mathbf{ksize}_M fixed in Fig. 11,
- for $\mathbf{ksize}_M = \mathbf{ksize}_{\text{GT}}$ in Fig. 10.

The sampling rate of the plotted curves increases towards the value boundaries of $\mathbf{t}_{\text{reg}}^{\text{peaks}}$. The results show:

- (1) **Varying ksize_{GT} for a fixed ksize_M , and the other way round, both have little influence on the performance.**
- (2) **Larger ksize_M have slight performance benefits** for common fixed ksize_{GT} . This may indicate a better noise robustness of larger kernel sizes. Larger kernel sizes can differentiate the quality of truth peaks in a larger range of peak sizes, boosting the influence of large interesting areas while decreasing that of small ones. Therefore, in the main paper we used the largest considered kernel size of 33, which also nicely fits typical body part proportions in the test dataset.
- (3) Fuzziness shows a consistent performance benefit (cf. precision-recall curves).
- (4) Increasing ksize_{GT} decreases the monitor precision. This is expected, as a higher ksize_{GT} also decreases the positive rate (cf. Tab. 8).

Table 8: Percentage of the 2693 MS COCO val2017 images with positive image-level ground truth annotations $\text{GT}_{\text{reg}}^{\text{peaks}}$ for different choices of ksize_{GT} and $\text{t}_{\text{GTreg}}^{\text{peaks}}$.

ksize_{GT}	$\text{t}_{\text{GTreg}}^{\text{peaks}}$	GT Pos. [%]
1	0.500	0.950
5	0.500	0.844
9	0.500	0.703
9	0.700	0.599
17	0.500	0.491
33	0.500	0.277

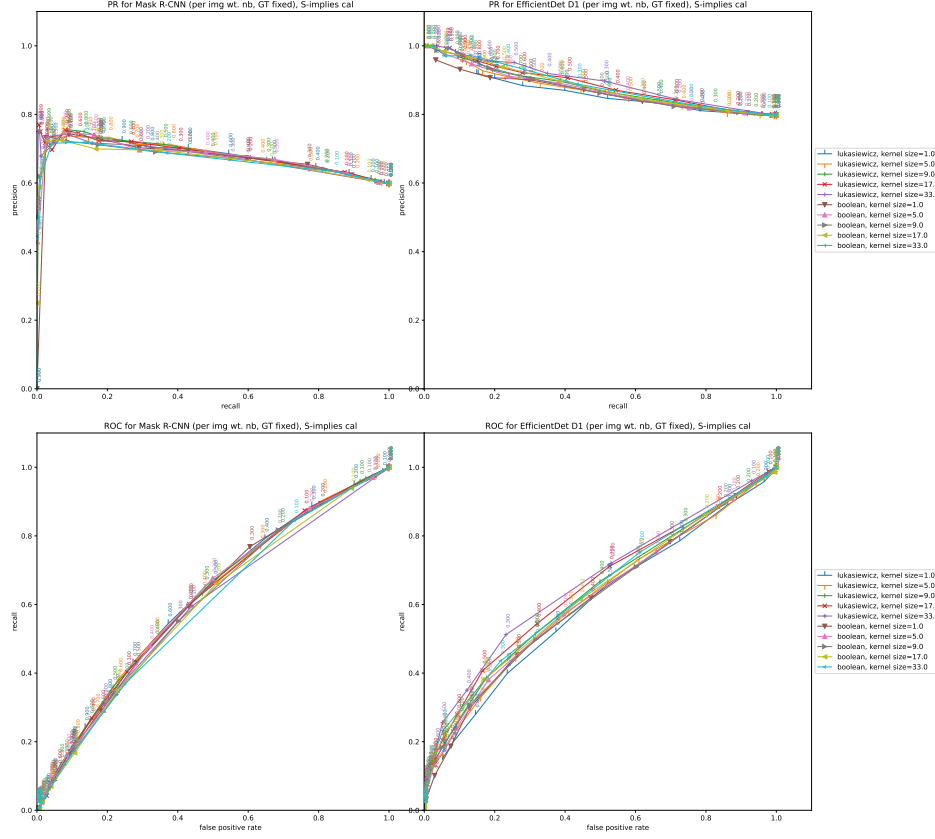


Fig. 9: Results for fixed $\text{ksize}_{\text{GT}} = 9$ and $\text{t}_{\text{GTreg}}^{\text{peaks}} = 0.7$. *Top*: Precision-recall curves, *bottom*: ROC curves over $\text{t}_{\text{reg}}^{\text{peaks}}$, *left*: Mask R-CNN, *right*: EfficientDet D1.

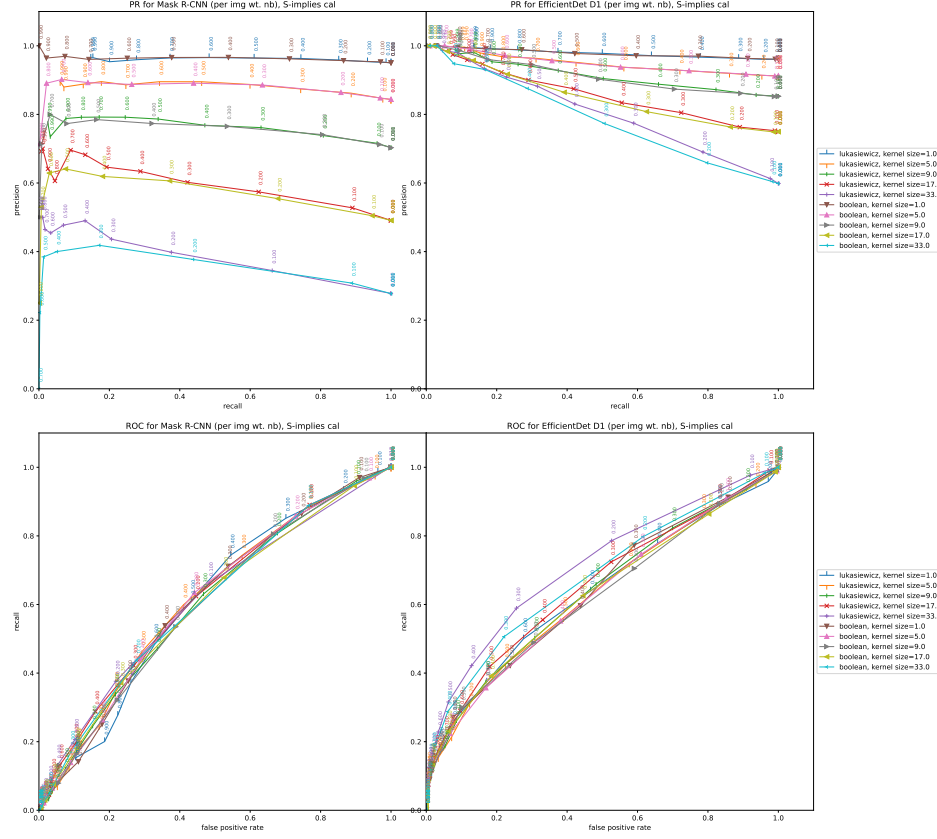


Fig. 10: Results for $\text{ksize}_M = \text{ksize}_{\text{GT}}$ and $\text{t}_{\text{GTreg}}^{\text{peaks}} = 0.5$. *Top*: Precision-recall curves, *bottom*: ROC curves over $\text{t}_{\text{reg}}^{\text{peaks}}$, *left*: Mask R-CNN, *right*: Efficient-Det D1.

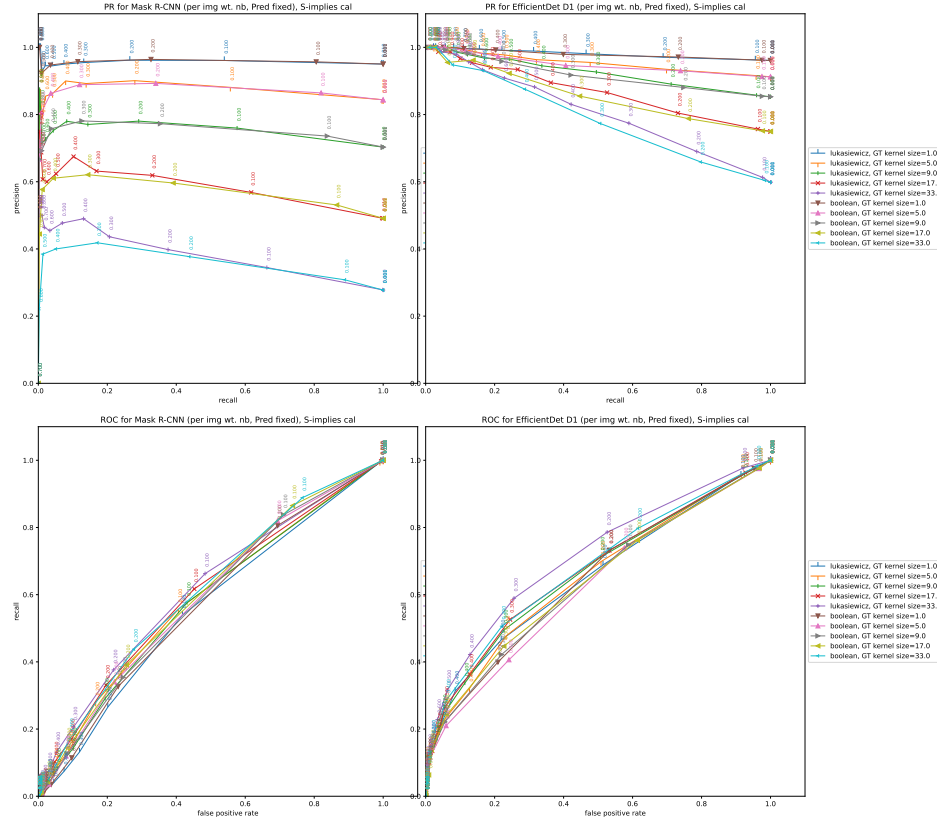


Fig. 11: Results for fixed $\text{ksize}_M = 33$ and $\tau_{\text{GTreg}}^{\text{peaks}} = 0.5$. *Top*: Precision-recall curves, *bottom*: ROC curves over $\tau_{\text{reg}}^{\text{peaks}}$, *left*: Mask R-CNN, *right*: Efficient-Det D1.